



**HAL**  
open science

# Considering syntrophic acetate oxidation and ionic strength improves the performance of models for food waste anaerobic digestion

Gabriel Capson-Tojo, Sergi Astals, Ángel Robles

► **To cite this version:**

Gabriel Capson-Tojo, Sergi Astals, Ángel Robles. Considering syntrophic acetate oxidation and ionic strength improves the performance of models for food waste anaerobic digestion. *Bioresource Technology*, 2021, 341, 10.1016/j.biortech.2021.125802 . hal-03777874

**HAL Id: hal-03777874**

**<https://hal.inrae.fr/hal-03777874>**

Submitted on 13 Aug 2023

**HAL** is a multi-disciplinary open access archive for the deposit and dissemination of scientific research documents, whether they are published or not. The documents may come from teaching and research institutions in France or abroad, or from public or private research centers.

L'archive ouverte pluridisciplinaire **HAL**, est destinée au dépôt et à la diffusion de documents scientifiques de niveau recherche, publiés ou non, émanant des établissements d'enseignement et de recherche français ou étrangers, des laboratoires publics ou privés.



Distributed under a Creative Commons Attribution - NonCommercial - NoDerivatives 4.0 International License

## Journal Pre-proofs

Considering syntrophic acetate oxidation and ionic strength improves the performance of models for food waste anaerobic digestion

Gabriel Capson-Tojo, Sergi Astals, Ángel Robles

PII: S0960-8524(21)01143-3

DOI: <https://doi.org/10.1016/j.biortech.2021.125802>

Reference: BITE 125802

To appear in: *Bioresource Technology*

Received Date: 8 July 2021

Revised Date: 12 August 2021

Accepted Date: 14 August 2021



Please cite this article as: Capson-Tojo, G., Astals, S., Robles, A., Considering syntrophic acetate oxidation and ionic strength improves the performance of models for food waste anaerobic digestion, *Bioresource Technology* (2021), doi: <https://doi.org/10.1016/j.biortech.2021.125802>

This is a PDF file of an article that has undergone enhancements after acceptance, such as the addition of a cover page and metadata, and formatting for readability, but it is not yet the definitive version of record. This version will undergo additional copyediting, typesetting and review before it is published in its final form, but we are providing this version to give early visibility of the article. Please note that, during the production process, errors may be discovered which could affect the content, and all legal disclaimers that apply to the journal pertain.

© 2021 Elsevier Ltd. All rights reserved.

1 **Considering syntrophic acetate oxidation and ionic strength improves the performance**  
2 **of models for food waste anaerobic digestion**

3 Gabriel Capson-Tojo <sup>a,b,\*</sup>, Sergi Astals <sup>c</sup>, Ángel Robles <sup>d</sup>

4  
5 <sup>a</sup> Advanced Water Management Centre, The University of Queensland, Brisbane, QLD 4072,  
6 Australia (E-mail: *g.capsontojo@uq.edu.au*)

7 <sup>b</sup> CRETUS, Department of Chemical Engineering, Universidade de Santiago de Compostela,  
8 15782 Santiago de Compostela, Galicia, Spain (E-mail: *gabriel.capsontoj@usc.es*)

9 <sup>c</sup> Department of Chemical Engineering and Analytical Chemistry, University of Barcelona,  
10 C/Martí i Franquès 1, 08028 Barcelona, Spain (E-mail: *sastals@ub.edu*)

11 <sup>d</sup> Department of Chemical Engineering, Universitat de València, Avinguda de la Universitat  
12 s/n, 46100 Burjassot, València, Spain (E-mail: *angel.robles@uv.es*)

13 \* Corresponding author: tel. +34 606.231.495, e-mail: *gabriel.capsontoj@usc.es*

14  
15 **Abstract**

16 Current mechanistic anaerobic digestion (AD) models cannot accurately represent the  
17 underlying processes occurring during food waste (FW) AD. This work presents an update of  
18 the Anaerobic Digestion Model no. 1 (ADM1) to provide accurate estimations of free ammonia  
19 concentrations and related inhibition thresholds, and model syntrophic acetate oxidation as  
20 acetate-consuming pathway. A modified Davies equation predicted NH<sub>3</sub> concentrations and pH  
21 more accurately, and better estimated associated inhibitory limits. Sensitivity analysis results  
22 showed the importance of accurate disintegration kinetics and volumetric mass transfer  
23 coefficients, as well as volatile fatty acids (VFAs) and hydrogen uptake rates. In contrast to the  
24 default ADM1, the modified ADM1 could represent methane production and VFA profiles  
25 simultaneously (particularly relevant for propionate uptake). The modified ADM1 was also

26 able to predict the predominant acetate-consuming and methane-producing microbial clades.  
27 Modelling results using data from reactors dosed with granular activated carbon showed that  
28 this additive improves hydrogen uptake.

29

### 30 **Keywords**

31 Anaerobic digestion; ADM1; Syntrophic acetate oxidation; Modelling; Ammonia inhibition

32

### 33 **1. Introduction**

34 Anaerobic digestion (AD) is a key technology for the sustainable management of several  
35 organic waste streams, including sewage sludge, food waste (FW), animal manure, agri-  
36 industrial waste, and industrial wastewater (Appels et al., 2008). AD is a multistage biochemical  
37 process that offers a triple role: (i) waste stabilization, (ii) production of renewable energy in  
38 the form of biogas, and (iii) nutrient recovery by digestate application. These benefits, together  
39 with new regulations penalizing cheaper alternatives (*i.e.* landfilling and incineration; European  
40 Directive 2018/850) and imposing circular economy action plans (European Commission  
41 Communication COM(2020)98), ensure a bright future for this biotechnology.

42 A clear example of the success of AD is the rapidly expanding treatment of concentrated wastes,  
43 such as FW or animal manure (Banks et al., 2008). The case of FW is particularly relevant, as  
44 its production is rapidly increasing due to population/economic growth, and policies imposing  
45 separate source selection and FW valorisation are being implemented (European Directive  
46 2008/98/CE). These factors call for developing sustainable processes that can provide efficient  
47 FW valorisation, with AD standing among the most suitable options (Capson-Tojo et al., 2016).  
48 AD mathematical modelling is well-established, and has largely been used for design purposes,  
49 operational analysis, technology development and process control (Regmi et al., 2019). The  
50 IWA Anaerobic Digestion Model no. 1 (ADM1), the most used AD model, is a mechanistic

51 model based on the underlying biological and physicochemical processes (Batstone et al., 2002;  
52 Weinrich and Nelles, 2021). The ADM1 was primarily developed to model sewage sludge AD  
53 in wastewater treatment plants. These digesters are characterised by relatively diluted solid  
54 concentrations (20-70 g TS·L<sup>-1</sup>; TS being total solids) and by relatively low risks of process  
55 inhibition and acidification (Appels et al., 2008; Astals et al., 2013). Accordingly, the default  
56 ADM1 is not able to accurately predict the performance of digesters treating concentrated  
57 organic streams or leading to high concentrations of inhibitors, such as ammonia. To overcome  
58 these limitations, several ADM1 modifications have been carried out in the last years. Relevant  
59 examples are the recent modifications of the ADM1 to consider variable mass/volume contents  
60 during high-solids AD (Pastor-Poquet et al., 2018), to account for non-ideal aqueous-phase  
61 chemistry (Patón et al., 2018; Solon et al., 2015), to include the syntrophic acetate oxidation  
62 (SAO) pathway (Montecchio et al., 2017; Rivera-Salvador et al., 2014), or to consider trace  
63 element (TE) complexation and precipitation (Flores-Alsina et al., 2016; Frunzo et al., 2019;  
64 Maharaj et al., 2019). As more research is carried out in AD, the knowledge on the underlying  
65 mechanisms governing the process increases, allowing to improve and modify models to  
66 accurately predict a broader spectrum of substrates, configurations, and operational conditions.  
67 A challenge in FW AD is free ammonia nitrogen (FAN) inhibition, caused by its high  
68 biodegradable protein concentrations and the low free water availability. High FAN  
69 concentrations cause inhibition of acetoclastic methanogenesis (AM; the predominant methane-  
70 producing pathway in digesters fed with sewage sludge). At FAN concentrations over 200-400  
71 mg FAN·L<sup>-1</sup>, hydrogenotrophic methanogenesis (HM) becomes predominant (Banks et al.,  
72 2012), coupled with SAO (Jiang et al., 2017). This two-step methane production process relies  
73 on acetate oxidation to CO<sub>2</sub> and H<sub>2</sub> by SAO bacteria, followed by their conversion into methane  
74 by hydrogenotrophic archaea. This process is only thermodynamically favourable at low H<sub>2</sub>  
75 partial pressures (10-80 Pa), and constant H<sub>2</sub> removal by hydrogenotrophic archaea is crucial

76 for making SAO energetically feasible (Rivera-Salvador et al., 2014). SAO has been already  
77 included into the ADM1, improving the model accuracy in digesters treating poultry litter and  
78 pretreated waste sludge (Montecchio et al., 2017; Rivera-Salvador et al., 2014).

79 AD processes dominated by SAO and HM are known to be prone to propionic acid  
80 accumulation, a major inhibitor in AD reactors (Banks et al., 2012). Syntrophic propionate  
81 oxidation (SPO) also requires low  $H_2$  partial pressures to be thermodynamically favourable,  
82 due to product-induced inhibition at high  $H_2$  levels. For the same reason, SPO also depends on  
83 the concentrations of acetic acid (Batstone et al., 2002; Capson-Tojo et al., 2017). Therefore,  
84 AD instabilities leading to increases in the  $H_2$  partial pressures can easily result in accumulation  
85 of acetic acid, which will further favour the accumulation of propionic acid. Because of its  
86 relevance, SPO is generally considered in mechanistic AD models (Batstone et al., 2002).

87 The high ionic strength in FW digesters causes another issue when considering traditional AD  
88 models, since the ion-pairing behaviour cannot be simplified to that of an ideal solution. Studies  
89 focusing on modelling ion speciation in concentrated AD systems have proved that assuming  
90 an ideal equilibrium can lead to overestimate FAN concentrations by up to 30% (Capson-Tojo  
91 et al., 2020; Hafner and Bisogni, 2009; Patón et al., 2018; Solon et al., 2015). Activity  
92 corrections have been applied to account for the effect of ionic strength on ion speciation,  
93 generally using the Davies equation for FAN quantification (Capson-Tojo et al., 2020; Patón et  
94 al., 2018; Solon et al., 2015). Despite its importance, this practice has been frequently omitted  
95 in the literature, even in publications devoted to FAN inhibition (Capson-Tojo et al., 2020;  
96 Rajagopal et al., 2013). FW digesters have the inherent risk of FAN inhibition and therefore a  
97 precise quantification of FAN is crucial to obtain coherent inhibitory limits that can be used to  
98 better predict process performance and inhibitory events (De Vrieze et al., 2015). The ADM1  
99 does not include the SAO pathway nor the effect of the ionic strength on ion speciation. This  
100 limits its applicability for FW AD, particularly in dry systems. These limitations are particularly

101 relevant as full-scale dry digesters (treating undiluted substrates with TS contents over 15%)  
102 are becoming more common worldwide (Karthikeyan and Visvanathan, 2013; Motte et al.,  
103 2013).

104 Recent modelling efforts on FW AD modelling have improved the ADM1 performance  
105 (Montecchio et al., 2019; Poggio et al., 2016; Rathnasiri, 2016). However, to the best of our  
106 knowledge, no previous publication on FW AD has assessed the impact of including SAO and  
107 media ionic strength on the ADM1 performance. Zhao et al. (2019) modified the ADM1 to  
108 account for FW composition, and calibrated relevant parameters after a sensitivity analysis.  
109 They concluded that hydrolysis, disintegration, and acetate uptake were the most influential  
110 processes on methane production. Zhao et al. (2019) did not assess the importance of FAN  
111 inhibition. Poggio et al. (2016) proposed a substrate characterisation methodology based on  
112 substrate fractionation to enhance the ADM1 performance. Hydrolysis was also identified as a  
113 relevant kinetic process, and two particulate fractions were needed to accurately model FW AD  
114 (*i.e.* a readily and a slowly particulate biodegradable fraction). Poggio et al. (2016) concluded  
115 that their approach led to good predictions for methane yields and solid destruction, being less  
116 accurate for the prediction of methane flow rates, pH and VFA profiles. Rathnasiri (2016)  
117 applied the ADM1 after FW dilution with water, and Montecchio et al. (2019) for FW co-  
118 digestion with sewage sludge, a co-substrate with lower N concentration and higher water  
119 content. Both approaches reduced the impact of TAN concentration on the digester  
120 performance, which eased fitting the experimental results with the default ADM1. Indeed,  
121 Montecchio et al. (2019) stated that the ADM1 was only adequate for AD at high bacterial and  
122 methanogenic activities (achieved when co-digesting FW and sludge).

123 The main goal of this study was to design a modified ADM1 able to accurately simulate FW  
124 AD. The ADM1 was modified to consider: (i) SAO as acetate-consuming pathway, (ii) FAN  
125 estimation using the Davies equation (to account for non-ideal behaviour), and (iii)

126 methanogenic inhibition due to FAN using a threshold inhibition function (Astals et al., 2018).  
127 The modified and default ADM1s were compared, considering their ability to predict both the  
128 AD performances and the predominant microbial communities. The influence of AD additives  
129 (e.g. granular activated carbon (GAC)) on the resulting model parameters was also assessed.

130

## 131 **2. Materials and methods**

### 132 *2.1. Inoculum source and substrate characteristics*

133 The inoculum was collected from a territorial-industrial plant in the South of France treating a  
134 mixture of different organic streams at high total ammonia nitrogen (TAN) concentrations ( $7.3$   
135  $\pm 0.5$  g N·L<sup>-1</sup>). FW was used as representative concentrated substrate. The FW was collected  
136 from different producers from the region of the Grand Narbonne (France). A proportional  
137 mixture (wet weight) of the different FWs was used as substrate. The characteristics of the FW  
138 and the inoculum, shown in Table 1, correspond to the average from two different FW sampling  
139 campaigns and to triplicate measurements for the inoculum.

### 140 *2.2. Batch anaerobic digestion*

141 Results from different sets of sequential batch digesters (with a working volume of  $430 \pm 2$  mL)  
142 treating FW were used as input data to calibrate and validate the default and the modified  
143 ADM1s (Capson-Tojo et al., 2018a). Data from the 2<sup>nd</sup> feeding of the sequential batch reactors  
144 was used to ensure proper inoculum adaptation and reactor operation. The digesters (in  
145 triplicate) were started with 60 g of FW as substrate (raw) at a substrate to inoculum ratio of 1  
146 g VS·g VS<sup>-1</sup> (with resulting FW concentrations of around 30 g VS FW·L<sup>-1</sup>; VS being volatile  
147 solids). The reactors were incubated at  $37 \pm 0.2$  °C. The incubation system was an Automated  
148 Methane Potential Testing System (AMPTSII) (Bioprocess Control, Sweden) consisting of 15  
149 parallel reactors with a total volume of 500 mL (of which 12 were used). To determine the  
150 methane flow rate, the headspace of each reactor was connected to a carbon dioxide trap (NaOH

151 5% solution) and then to a gas flow meter. The reactors were automatically stirred for 1 minute  
152 every 10 minutes at 40 rpm. Before starting the incubation, the headspace was flushed with  
153 pure N<sub>2</sub> to ensure anaerobic conditions. To account for endogenous respiration, a blank reactor  
154 containing only inoculum was also run (in triplicate). The methane production from the blank  
155 was subtracted from the biogas produced by the reactors fed with FW. The batches were stopped  
156 after 34 days, once the biogas production stopped in all reactors, and the total volatile fatty acids  
157 (VFAs) concentration was assumed to be negligible.

158 To assess the applicability of the proposed model modifications, data from reactors working  
159 under different conditions were used: (i) control conditions (solely fed with FW), and (ii)  
160 supplemented with GAC (dosed at 10 g·L<sup>-1</sup>). A detailed explanation of the experimental design  
161 and the sampling procedure can be found in Capson-Tojo et al. (2018a).

### 162 2.3. Analytical methods

#### 163 2.3.1. Physicochemical characterization of the FW

164 TS and VS contents were measured according to the standard methods of the American Public  
165 Health Association (APHA, 2017). Carbohydrate contents were determined using the Dubois  
166 method (Dubois et al., 1956), and lipid contents via accelerated solvent extraction using an  
167 ASE®200, DIONEX (California, United States of America) coupled to a MULTIVAPOR P-12,  
168 BUCHI (Aqun, Netherlands) with heptane as solvent (100 bar, 105 °C, 5 cycles of 10 min  
169 static and 100 s purge) (APHA, 2017). Total Kjeldahl Nitrogen (TKN) contents were  
170 determined with an AutoKjeldahl Unit K-370, BUCHI, and the protein contents were estimated  
171 from TKN values using a factor of 6.25 g protein·g organic N<sup>-1</sup> (Galí et al., 2009). The pH was  
172 measured using a WTW (London, United Kingdom) pHmeter series inoLab pH720. The FW  
173 biochemical methane potential (BMP) was determined according to Motte et al. (2014),  
174 following Angelidaki et al. (2009). The chemical oxygen demand (COD) content of the FW  
175 was estimated from the contents in carbohydrates (1.19 g COD·g<sup>-1</sup>), proteins (1.42 g COD·g<sup>-1</sup>)

176 and lipids (2.90 g COD·g<sup>-1</sup>), assuming a 10% of inert COD (based on Batstone et al., (2002),  
177 and from the FW biodegradability estimated from the BMPs, of 92%).

### 178 2.3.2. Analysis of metabolites, final products, and microbial communities

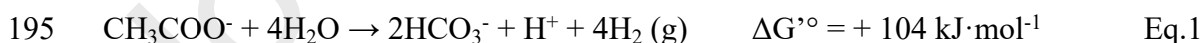
179 A plastic tube connected to the cover of each AMPTSII reactor enabled digestate sampling  
180 without modifying the composition of the gas in the headspace. Samples (5-10 mL) were taken  
181 approximately every 2 days, with a total of 15 samples per reactor taken during the duration of  
182 the experiments. The concentrations of volatile fatty acids (VFAs) and ionic species (*i.e.* TAN,  
183 PO<sub>4</sub><sup>3-</sup>, Na<sup>+</sup>, or K<sup>+</sup>) in the digestates were analysed by gas and ion chromatography, as described  
184 in Motte et al. (2013). The product yields were corrected to account for the digestate removed,  
185 by accounting for the mass of substrate removed in every sampling.

186 The methane flow rates were quantified using CO<sub>2</sub> traps and gas flow meters connected to the  
187 headspace of the reactors. The microbial communities at the beginning and the end of the tests  
188 were analysed via 16S rRNA sequencing (MiSeq), as described in Moscoviz et al. (2017).

### 189 2.4. ADM1 modifications

#### 190 2.4.1. Syntrophic acetate oxidation

191 SAO was included into the ADM1 following a similar approach to that presented in Rivera-  
192 Salvador et al. (2014). Stoichiometry was set according to Equation 1, and Monod kinetics were  
193 applied for SAO. As in Rivera-Salvador et al. (2014), hydrogen inhibition in acetate uptake by  
194 SAO was considered using a non-competitive inhibition function.



#### 196 2.4.2. FAN quantification using a modified Davies equation

197 The FAN concentrations were calculated using the modified Davies equation proposed in  
198 Capson-Tojo et al. (2020). This approach considers the pH, temperature and I of the media,  
199 introducing an activity coefficient (*f*) as correction factor into the ideal equilibrium equation,  
200 resulting in Equation 2 (Stumm and Morgan, 1996). The set of expressions used is as follows:

$$201 \quad FAN = \frac{K_a \cdot f \cdot TAN}{K_a \cdot f + 10^{-pH}} \quad \text{Eq. 2}$$

$$202 \quad f = 10^{\left(-A \cdot z_i^2 \cdot \left(\frac{\sqrt{I}}{1 + \sqrt{I}}\right) - \lambda \cdot I\right)} \quad \text{Eq. 3}$$

$$203 \quad A = 1.82 \cdot 10^6 \cdot (\varepsilon \cdot T)^{-\frac{3}{2}} \quad \text{Eq. 4}$$

$$204 \quad I = \frac{1}{2} \sum_{i=1}^n C_i \cdot z_i^2 \quad \text{Eq. 5}$$

205 Where  $K_a$  is the acid-base equilibrium constant,  $I$  is the ionic strength (M),  $\lambda$  is an empirically  
 206 determined constant (0.1276 according to Capson-Tojo et al. (2020)),  $\varepsilon$  is the dielectric constant  
 207 of water at the working temperature (74.828 and 68.345 at 35 and 55 °C, respectively),  $C_i$  is the  
 208 concentration of the species  $i$  (M),  $T$  is the temperature, and  $z_i$  is the corresponding charge.

#### 209 2.4.3. FAN threshold inhibition function

210 The inhibition function considered for FAN inhibition on methanogenic archaea was the  
 211 threshold inhibition function proposed by Astals et al. (2018):

$$212 \quad I_{FAN} = \begin{cases} 0 & ; \text{if } FAN \leq K_{I,NH3,min} \\ 1 - e^{-2.77259 \left(\frac{FAN - K_{I,NH3,min}}{K_{I,NH3,max} - K_{I,NH3,min}}\right)^2} & ; \text{if } FAN > K_{I,NH3,min} \end{cases} \quad \text{Eq. 6}$$

213 Where  $I_{FAN}$  is the inhibition factor related to the presence of FAN,  $K_{I,NH3,min}$  and  $K_{I,NH3,max}$  are  
 214 the FAN concentrations where inhibition starts (onset concentration) and when it is almost  
 215 complete (specific methanogenic activity (SMA) =  $0.06 \cdot SMA_{max}$ ), respectively (Astals et al.,  
 216 2018). The constant 2.77259 ensures that the midpoint between  $K_{I,NH3,min}$  and  $K_{I,NH3,max}$  equals  
 217  $K_{I,NH3}$  (FAN 50% inhibitory concentration for acetate uptake by methanogens).

218 The threshold function provides a more accurate representation of the impact of FAN on AM  
 219 activity, and it allows to identify a lower and an upper inhibition limit (Astals et al., 2018). This  
 220 inhibition function allows defining precise thresholds that can serve to simulate changes in the  
 221 predominant methanogenic pathways according to the FAN concentrations.

#### 222 2.4.4. Accounting for the different dynamics of butyrate and valerate consumption

223 The modified ADM1 uncoupled the uptake of butyrate and valerate by adding a new bacterial  
224 group responsible for valerate uptake ( $X_{c5}$ ). In this approach,  $X_{c4}$  were only responsible for the  
225 uptake of butyrate (opposed to the ADM1, where  $X_{c4}$  consume both butyrate and valerate). The  
226 competitive term originally present in the default ADM1 was removed in the rate equations for  
227 butyrate and valerate uptake. This approach was implemented in previous models also dealing  
228 with high-solids AD, aiming at obtaining an accurate representation of the different kinetics of  
229 butyrate and valerate uptake (Pastor-Poquet et al., 2019, 2018).

### 230 *2.5. Model calibration and evaluation*

231 To compare the models (*i.e.* default *vs.* modified ADM1s) and to evaluate the effects of GAC  
232 on the AD performance (see Section 2.2), a systematic approach was followed. First, a global  
233 sensitivity analysis (GSA) was carried out for each model to identify influential parameters on  
234 the model outputs. Afterwards, these parameters were dynamically calibrated to improve the  
235 prediction capabilities of the models and to compare between the different experimental  
236 conditions (*i.e.* control *vs.* GAC-dosed reactors). The required stoichiometric parameters,  
237 biomass compositions, biomass yields, and physicochemical parameters were all obtained from  
238 the literature, as well as the initial values of the kinetic parameters (Batstone et al., 2002;  
239 Capson-Tojo et al., 2020; Rivera-Salvador et al., 2014; Rosen and Jeppsson, 2006). We are  
240 willing to share the code files corresponding to both the default and the modified ADM1s  
241 (implemented in MATLAB® (MATLAB R2021a, The MathWorks Inc., Natick, MA, USA)).

#### 242 *2.5.1. Sensitivity analysis*

243 The GSA methodology implemented was similar to the one described in Robles et al. (2014),  
244 based on the Morris screening Method (Morris, 1991). This approach consists in a one-factor-  
245 at-a-time method of GSA, which evaluates the distribution of the scaled elementary effects of  
246 each input factor (model parameters) upon model outputs (methane production rates and VFAs  
247 concentration), which is afterwards used to calculate the statistical parameters that provide

248 sensitivity data. The variation for each input factor was set to  $\pm 20\%$  of the default value, through  
 249 a resolution of 4  $p$  levels. The number of evaluated trajectories was 100. The absolute mean  
 250 ( $\mu^*$ ) and the standard deviation ( $\sigma$ ) of the scaled elementary effects of each distribution were  
 251 used as sensitivity measures (Campolongo et al., 2007). The graphical Morris approach was  
 252 used to systematically differentiate between input factors that could significantly influence the  
 253 model. The  $\mu^*$  and  $\sigma$  obtained for all the scaled elementary effects of each distribution were  
 254 plotted. Factors with high  $\mu^*$  and (relatively) small  $\sigma$  were considered to be influential, with  
 255 linear and additive effects on the outputs. Factors with small  $\mu^*$  but high  $\sigma$  were considered to  
 256 be influential, with non-linear or interactive effects on the outputs. Factors with low  $\mu$  and  $\sigma$   
 257 were considered as non-influential (Morris, 1991).

#### 258 2.5.2. Dynamic calibration of the model

259 The parameters considered as influential from the GSA results were dynamically calibrated by  
 260 adjusting the relevant simulated data (*i.e.* methane production rates and VFA concentrations)  
 261 to the experimental results. A global constrained optimization was conducted using a genetic  
 262 algorithm (MATLAB R2021a). Bound constrains for variations of model inputs were set to  
 263  $\pm 95\%$  of default values, except for pH-related inhibition parameters ( $\pm 10\%$ ). The objective  
 264 function to be minimised (standardized residuals) is shown in Eq. 7, where  $X_{SIM}$  and  $X_{EXP}$  are  
 265 the simulated and measured values for each variable  $i$ . No ponderation factors were applied.

$$266 \quad \sum_{i=1}^n \left( \frac{|X_{SIM_i} - X_{EXP_i}|}{\sqrt{\text{std}(X_{EXP_i})}} \right) \quad (\text{Eq. 7})$$

267

### 268 3. Results and discussion

#### 269 3.1. Comparison of the resulting models after sensitivity analysis and calibration

##### 270 3.1.1. Results from global sensitivity analysis

271 The graphical outputs from the GSA for both the default and the modified ADM1 for the control

272 reactor are shown in Fig. 1. Regarding the methane production rates ( $Q_{\text{CH}_4}$ ), the results of both  
273 models (Figs. 1A and 1F) showed that the most relevant parameters were all related to acetate  
274 uptake (e.g. AM or SAO maximum specific uptake rates ( $k_m$ ), and AM inhibition parameters,  
275 either  $K_{\text{I,NH}_3}$  or  $K_{\text{I,NH}_3,\text{max,acet}}$  ( $K_{\text{I,NH}_3,\text{max}}$  for acetotrophs) depending on the model). The  
276 disintegration and decay first order rate constants ( $k_{\text{dis}}$  and  $k_{\text{dec}}$ ) and the volumetric mass transfer  
277 coefficient ( $k_{\text{L}}a$ ) also appeared as relevant. The acetate-uptake related parameters (i.e.  $k_{\text{m,ac}}$  and  
278  $k_{\text{m,SAO}}$ ) illustrate the predominance of this VFA as main methane-producing intermediate  
279 metabolite, which is in agreement with FW AD literature (Capson-Tojo et al., 2017; Jiang et  
280 al., 2017). The relevance of  $k_{\text{dis}}$  and  $k_{\text{L}}a$  is explained by the high contents of solids in the reactors  
281 (the high TS contents in FW, around 20%, often lead to TS contents of 5%). With most of the  
282 organic matter being present as particles, their disintegration appears as a critical process,  
283 potentially acting as rate limiting step. Furthermore, the high TS contents and consequent lack  
284 of water also affect gas transfer and diffusion, reason why the  $k_{\text{L}}a$  is important.

285 The model structure also affected the results, with SAO-related parameters (i.e.  $k_{\text{m,SAO}}$ )  
286 appearing as relevant in the modified ADM1. Both models showed again similar results  
287 regarding the uptake of acetate (Figs. 1B and 1G), with parameters related to acetate uptake  
288 being deemed as relevant (AM or SAO uptake kinetic parameters, or AM inhibition  
289 parameters). SAO-related parameters were also relevant in the modified ADM1, confirming the  
290 importance of this pathway. The uptake of other VFAs (i.e. propionate, butyrate, and valerate;  
291 Figs. 1C-E and 1H-J) was governed by the respective Monod kinetic parameters (i.e.  
292 corresponding  $k_m$  and  $K_S$ ;  $K_S$  being the saturation constant) and by parameters related to  
293 hydrogen uptake (e.g. hydrogen uptake parameters and corresponding inhibitory terms for each  
294 VFA). In the modified ADM1,  $k_{\text{dis}}$  was also found relevant, due to the solid nature of FW.

### 295 3.1.2. Model calibration and comparison of prediction capabilities: default vs. modified ADM1

296 The parameters deemed as relevant according to the GSA were calibrated using both models

297 and the control reactor dataset (as in Section 3.1.1). The GSA allowed to reduce the number of  
298 parameters to calibrate from an initial set of 31 in the default ADM1 and 41 in the modified  
299 ADM1, to 13 and 16, respectively. The calibration results are shown in Table 2.

300 The parameters deemed as relevant for methane production and/or VFA uptake were selected  
301 for calibration. Despite the influence of  $\text{pH}_{\text{UL,ac}}$  (pH upper limit for acetotrophs) on the resulting  
302 methane flow rates and acetate uptake rates (see Fig. 1),  $\text{pH}_{\text{UL,ac}}$  and  $\text{pH}_{\text{LL,ac}}$  (pH lower limit for  
303 acetotrophs) were excluded from the calibration of the modified ADM1. pH-related inhibition  
304 parameters were deemed as relevant by the GSA because, mathematically, AM can be inhibited  
305 by modifying the pH inhibition limits. Nevertheless, the resulting calibrated values leading to  
306 AM inhibition by pH were 8.0-8.5 for  $\text{pH}_{\text{LL,ac}}$  and over 9.0 for  $\text{pH}_{\text{UL,ac}}$ , which biologically do  
307 not make sense (Batstone et al., 2002). Therefore, including these parameters in the calibration  
308 procedure resulted in illogical inhibition limits, affecting the values of other parameters and  
309 leading to inaccurate results. Furthermore, using the default ADM1, the calibrated values for  
310  $\text{pH}_{\text{UL,ac}}$  were 6.4-7.1, which agree with values reported in the literature (Batstone et al., 2002).  
311 The calibration results showed that FW has a relatively fast disintegration kinetics ( $>0.6 \text{ d}^{-1}$ )  
312 compared to other solid substrates, with values of  $k_{\text{dis}}$  higher than those reported in the literature  
313 (e.g.  $0.24 \text{ d}^{-1}$  for cattle manure or  $0.10 \text{ d}^{-1}$  for pig manure (Batstone et al., 2002)). This result is  
314 in agreement with the well-known faster disintegration and hydrolysis of FW (Koch et al.,  
315 2015). The much lower values of  $k_{\text{LA}}$  when compared to the literature are related to the lack of  
316 water and the inherent difficult mixing at high solid contents.

317 To understand the resulting values of the kinetic parameters for each model, their prediction  
318 performances and the predicted dominant pathways must be analysed in detail. The modelling  
319 results are presented in Fig. 2 (methane flow rates and VFA profiles) and Fig. 3 (biomass  
320 concentrations, and pH and TAN/FAN concentrations). As shown in Fig. 2, while both models  
321 represented accurately the acetate and total VFA profiles (parity plots with  $R^2$  of 0.98-0.99),

322 the calibrated default ADM1 was not able to represent the methane production rate ( $R^2$  of 0.61)  
323 nor the final consumption of propionate (see Fig. 2). In contrast, the modified ADM1 provided  
324 more accurate predictions in both cases ( $R^2$  of 0.94 and 0.99, respectively).

325 The improved predicting capabilities of the modified ADM1 are related to the underlying  
326 processes governing AD in each model. In the default ADM1, AM is the only acetate-  
327 consuming pathway available. Therefore, to fit the experimental methane production rates and  
328 the total VFA and acetate profiles, the FAN inhibitory concentrations for acetoclastic archaea  
329 ( $K_{I,NH_3}$ ) need to be far above commonly applied inhibitory concentrations (*e.g.*  $K_{I,NH_3}$  values of  
330 at 0.0030 vs. 0.0018 M (Batstone et al., 2002)). In contrast, the calibration results with the  
331 modified ADM1 showed a realistic FAN inhibitory limit for acetoclastic archaea (*i.e.* a  
332  $K_{I,NH_3,max,acet}$  of 0.011 M, as in Capson-Tojo et al. (2020)). This value led to inhibition of AM,  
333 which can be confirmed when looking at the predicted concentrations of methanogenic archaea  
334 (Fig. 3). Therefore, SAO was the main acetate-consuming pathway, and HM the main methane-  
335 producing one, which is in agreement with the experimental results (where the presence of  
336 acetoclastic archaea at the end of the batch tests was negligible, see Capson-Tojo et al. (2018a)  
337 for a detailed discussion on the microbial communities in the reactors). The accurate  
338 representation of the underlying microbial processes by the modified ADM1 was facilitated by  
339 including SAO as metabolic pathway, and by using realistic FAN inhibitory limits for  
340 acetoclastic archaea. These allowed to account for the observed AM inhibition, resulting in the  
341 dominance of SAO (and HM) despite their slower overall kinetics. The low concentrations of  
342 syntrophic bacteria predicted by the modified ADM1 are caused by their slow growth, generally  
343 representing a minor part of the total microbial community in digesters (Hao et al., 2020). These  
344 results agree with previous studies dealing with SAO during AD at high N concentrations.  
345 Hydrogenotrophic methanogens were also dominant in thermophilic AD of poultry litter  
346 (Rivera-Salvador et al., 2014), and Montecchio et al. (2017) did not detect any acetoclastic

347 archaea in their reactors treating sludge at  $0.3 \text{ g FAN}\cdot\text{L}^{-1}$ .

348 The different predominant methanogenic pathways between both models explain the inability  
349 of the default ADM1 to predict the methane production rates. The high  $\text{H}_2$  concentrations  
350 occurring during FW AD can potentially make thermodynamically unfavourable the processes  
351 in which  $\text{H}_2$  was produced, such as SAO, propionate oxidation, butyrate oxidation, and valerate  
352 oxidation (accounted for in both models by the 50% inhibitory concentrations of  $\text{H}_2$ ,  $K_{i,\text{H}_2}$ ).

353 This can lead to the accumulation of VFAs often seen in full-scale FW digesters (Banks et al.,  
354 2012; Capson-Tojo et al., 2017). In the case of propionate, butyrate, and valerate, high acetate  
355 concentrations might further inhibit their consumption (see Batstone et al. (2002) and Capson-  
356 Tojo et al. (2017) for a deeper discussion on AD thermodynamics). As the modified ADM1  
357 included SAO and HM, it was able to predict high  $\text{H}_2$  concentrations and partial pressures in  
358 the reactor, thus accurately predicting VFA accumulation. The default ADM1 could not predict  
359 an AD system dominated via SAO and HM, and thus could not predict the consequent high  $\text{H}_2$   
360 concentrations and the resulting VFA accumulation. Therefore, to represent the VFA profiles,  
361 the calibration procedure decreased the  $k_{\text{L}a}$  value in the default ADM1 to values allowing the  
362 high  $\text{H}_2$  concentrations required. The  $k_{\text{L}a}$  estimated by the default ADM1 was much lower than  
363 the one obtained with the modified ADM1 ( $0.087$  and  $0.390 \text{ d}^{-1}$ , respectively). The low  $k_{\text{L}a}$   
364 value resulted in the accumulation of, not only  $\text{H}_2$ , but also  $\text{CH}_4$ , reason why the methane  
365 production rates could not be predicted by the default ADM1.

366 The phenomena described above can also explain the resulting  $k_{\text{m}}$  values. Regarding acetate,  
367 the default ADM1 needed a high  $k_{\text{m},\text{ac}}$  value of  $10.7 \text{ g COD}\cdot\text{g COD}^{-1}\cdot\text{d}^{-1}$ , while the value in the  
368 modified ADM1 was  $1.30 \text{ g COD}\cdot\text{g COD}^{-1}\cdot\text{d}^{-1}$ , as SAO was the dominant acetate-consuming  
369 pathway. AM was irrelevant in the modified model (see Fig. 3B), leading to biased values of  
370  $k_{\text{m},\text{ac}}$ . Similarly, the less pronounced  $\text{H}_2$ -induced inhibition predicted by the default model (due  
371 to lower  $\text{H}_2$  concentrations as HM was marginal) resulted in a very low value of  $k_{\text{m}}$  for

372 propionate uptake ( $2.93 \text{ g COD} \cdot \text{g COD}^{-1} \cdot \text{d}^{-1}$ , far from literature values) to reproduce the  
373 propionate accumulation observed experimentally. In contrast, the  $k_m$  for propionate uptake in  
374 the modified ADM1 ( $19.2 \text{ g COD} \cdot \text{g COD}^{-1} \cdot \text{d}^{-1}$ ) was within ranges commonly reported in the  
375 literature (Batstone et al., 2002). Regarding the  $\text{H}_2$  uptake rates, the values in the modified  
376 ADM1 allowed a simultaneous, syntrophic growth of hydrogenotrophic archaea and SAO (Fig.  
377 3B). The higher values of  $k_m$  in the default ADM1 resulted in an initial fast  $\text{H}_2$  consumption,  
378 followed by the death of hydrogenotrophic archaea (Fig. 3A). This allowed to reduce the initial  
379  $\text{H}_2$  concentrations to values where there was no VFA accumulation. Nevertheless, as in the  
380 default ADM1 SAO did not occur, less  $\text{H}_2$  was predicted than in the modified ADM1, which  
381 jeopardised the simultaneous representation of methane production rates and VFA profiles.

382 Butyrate and valerate uptake were separated into two different processes in the modified  
383 ADM1, aiming at accurately representing their profiles. This strategy allowed setting different  
384 uptake dynamics for each clade, as it was obvious from the experimental data that they had  
385 different dynamics (more butyrate was initially generated than valerate, butyrate was produced  
386 faster, and valerate consumption was slower). Despite these efforts, both models failed to  
387 accurately predict the valerate profile ( $R^2$  of 0.74-0.82). The most plausible explanation is that  
388 other processes were taking place, affecting both butyrate and valerate concentrations. Several  
389 biological reactions involve these compounds as substrate or products, and relevant processes  
390 such as chain elongation are known to occur during fermentation or AD of FW (Capson-Tojo  
391 et al., 2018b). Nonetheless, the low concentrations of valerate during FW AD ( $< 5\%$  of the total  
392 COD as products) justify the omission of other involved processes. If an accurate prediction of  
393 valerate concentrations in the future is needed, further research should be carried out.

394 Another difference between the default and the modified ADM1 is the method used for FAN  
395 quantification and FAN-related inhibition. These differences affected the predicted pH profiles  
396 (more accurate in the modified ADM1), and thus also the FAN concentrations, which the

397 default ADM1 underestimated by up to 55% (Figs. 3C and 3D). This underestimated FAN  
398 concentrations imply that, under a correct FAN calculation, the calibrated value of  $K_{I,NH_3}$  in the  
399 default ADM1 would be considerably higher than those presented in Table 2, leading to even  
400 less realistic values. It must be considered that these differences between the predicted FAN  
401 concentrations are not only a consequence of the different pH values, but also of including the  
402 ionic strength in the FAN concentration estimation procedure.

### 403 3.2. Model application: using the modified ADM1 to explain the effect of AD additives

404 Carbon conductive materials have been reported to enhance the performance of AD reactors,  
405 particularly in FAN-rich digesters (Barua and Dhar, 2017). Improvements due to GAC addition  
406 have been related to: (i) allowing direct interspecies electron transfer (DIET) (Barua and Dhar,  
407 2017); (ii) the formation of biofilms on its surface (Fagbohunge et al., 2017); (iii) the sorption  
408 of inhibitors onto its surfaces (Fagbohunge et al., 2017); and (iv) an increased buffering  
409 capacity (Barua and Dhar, 2017). Bioprocess modelling has never been used to increase our  
410 understanding on this topic, likely because available models did not include some of the  
411 relevant metabolic pathways occurring in the reactors.

412 The modified and default ADM1s were calibrated over experiments supplemented with GAC  
413 (after inoculum adaptation in sequential batch reactors). The calibration and modelling results  
414 are shown in Table 3 and Fig. 4, respectively. The modified ADM1 was able to represent the  
415 total VFA, acetate, and propionate profiles, and the methane production rates ( $R^2$  values from  
416 parity plots of 0.93-0.99). As previously, butyrate and valerate concentrations were predicted  
417 less accurately. The default ADM1 showed the same limitations found with the control reactor,  
418 with barely any methane production ( $R^2$  of 0.16) due to an extremely low  $k_{La}$  value. For both  
419 models, the corresponding FAN inhibition constants and predicted biomass concentrations (not  
420 shown, similar to those in Fig. 3) confirmed the predominant pathways described for the control  
421 reactor, *i.e.* SAO and HM being dominant in the modified ADM1 and AM in the default ADM1

422 (see Table 3 for inhibitory constants).

423 The calibration results (Table 3) show that GAC addition significantly enhanced the H<sub>2</sub> uptake  
424 kinetics ( $k_{m,H_2}$  of 4.7 g COD·g COD<sup>-1</sup>·d<sup>-1</sup> in the control reactor and of 24 g COD·g COD<sup>-1</sup>·d<sup>-1</sup>  
425 in the GAC dosed reactor), which resulted in a faster uptake of the other VFAs due to a lower  
426 H<sub>2</sub> partial pressure. The kinetics of SAO, propionate, butyrate, or valerate uptake were not  
427 directly enhanced by GAC addition. These results suggest that the improvement observed in  
428 AD performance after GAC addition is mainly due to a faster HM kinetics. This can be a  
429 consequence of biofilm formation onto the GAC particles, thus favouring syntrophic  
430 interactions. Another explanation could be the occurrence of DIET, which is a faster electron  
431 transfer mechanism than mediated transport. As single electrons are not a state variable in the  
432 model, DIET would simply be translated in the model as a faster HM process. These  
433 mechanisms have been further discussed in Capson-Tojo et al. (2018a). Opposed to these  
434 findings, the calibration results using the default ADM1 (Table 3) would explain these  
435 enhancements via increasing the AM and SPO rates. As microbial community analyses showed  
436 that the relative abundance of AM in the reactors was negligible, the default ADM1 would have  
437 led to misleading conclusions.

438 These results show that the modified ADM1 can be applied to further understand the underlying  
439 processes governing FW AD. The application shown here indicates that the modified ADM1  
440 can be used to explain the positive effects that AD additives have on the process kinetics,  
441 allowing to identify the processes that are more significantly affected.

### 442 *3.3. Comparison of the obtained parameters with literature values*

443 The parameters from the default ADM1 agree with those reported by other studies modelling  
444 FW without including SAO. Zhao et al. (2019) targeted  $k_{dec}$ ,  $k_{dis}$ ,  $k_{hyd,ch}$ ,  $k_{m,ac}$ , and  $K_{S,ac}$  for  
445 calibration due to their significant influence on methane production. The recommended  
446 calibration values were 0.001 g COD·g COD<sup>-1</sup>·d<sup>-1</sup>, 0.16 g COD·g COD<sup>-1</sup>·d<sup>-1</sup>, 3 g COD·g

447 COD<sup>-1</sup>·d<sup>-1</sup>, 1 g COD·g COD<sup>-1</sup>·d<sup>-1</sup>, and 0.23 mg COD·L<sup>-1</sup>, respectively. The values of these  
448 parameters for both models (presented in Tables 2 and 3;  $k_{m,ac}$ , and  $K_{S,ac}$  only for the default  
449 ADM1) are within the ballpark of those previously reported, confirming their applicability (see  
450 values from the control reactor for less biased comparisons). The obtained  $k_{dis}$  values are also  
451 close to those recommended in the ADM1 for food waste, of 0.41 d<sup>-1</sup> (Batstone et al., 2002).  
452 Regarding inhibitory parameters, values of  $K_{I,NH_3}$  up to 0.0028 M have been used for AD of the  
453 organic fraction of municipal solid waste (Pastor-Poquet et al., 2019). As the values obtained  
454 in this article (up to 0.0035 M), a  $K_{I,NH_3}$  of 0.0028 M is much higher than the common inhibitory  
455 limit applied in the default ADM1 (0.0018 M). However, it must be considered that the default  
456 ADM1 was designed for modelling AD of dilute sewage sludge (TS <5%) from wastewater  
457 treatment plants, with lower FAN concentrations, thus representing microbial communities  
458 unadapted to high FAN concentrations. The corresponding inhibitory limit to be used for FAN-  
459 adapted processes (applied in our modified model) has been estimated around 0.0057 M  
460 (corresponding to values of  $4.3 \cdot 10^{-4}$  M and 0.0109 M for  $K_{I,NH_3,min,acet}$  and  $K_{I,NH_3,max,acet}$  in the  
461 threshold function) (Capson-Tojo et al., 2020).

462 The results from sensitivity analyses and model calibrations carried out in previous publications  
463 including SAO also agree with those presented in Tables 2 and 3 for the modified ADM1  
464 (Montecchio et al., 2017; Rivera-Salvador et al., 2014). In previous publications, the kinetic  
465 parameters (*e.g.* uptake rates) related to SAO and HM were found to be relevant (Montecchio  
466 et al., 2017; Rivera-Salvador et al., 2014). For comparison purposes, Table 4 shows the values  
467 of the uptake rates for acetate-uptake related processes (*i.e.* AM and SAO) and for HM, from  
468 the literature and from this study. It must be considered that the data used in this work (and in  
469 most of the studies presented in Table 4) was obtained from batch reactors. Therefore, the initial  
470 biomass concentrations influenced to some extent the values of the obtained kinetic parameters.  
471 It is important to consider that most previous AD models including SAO omitted AM, thus

472 excluding potential interactions between competing pathways (Montecchio et al., 2017; Rivera-  
473 Salvador et al., 2014). The modified ADM1 presented here considers both AM and SAO, which  
474 means that microbial competitions and shifts can be modelled by considering environmental  
475 factors (*e.g.* FAN concentration). To the best of our knowledge, only Wett et al. (2014)  
476 implemented both AM and SAO simultaneously, but they did not discuss competitions between  
477 them, neither their inhibition under different conditions. In practice, Wett et al. (2014) virtually  
478 omitted AM, since the  $k_m$  values were extremely low ( $0.3 \text{ kg COD} \cdot \text{kg COD}^{-1} \cdot \text{d}^{-1}$ , see Table 4).

#### 479 *3.4. Implications for industrial application and further model development*

480 This work shows that to properly model FW AD, key modifications must be made to the default  
481 ADM1 (*i.e.* including SAO and the impact of ionic strength on ion speciation). These  
482 modifications are important for the accurate prediction of the performances of digesters treating  
483 FW, which otherwise could not be achieved (*e.g.* inaccurate biogas production rates and/or  
484 acetate and propionate concentrations in the digesters by the default ADM1). In FW AD, VFAs  
485 accumulation is responsible for low performance, or even reactor failure. Their accurate  
486 prediction is crucial to understand the behaviour of these systems, to improve digester design,  
487 and to better assess mitigation strategies.

488 The accurate representation of methane and the VFA profiles has direct implications for  
489 optimisation of operational parameters (*e.g.* loading rates and retention times), for simulating  
490 scenarios with different co-substrates (*e.g.* predicting the impact of introducing a new waste  
491 stream into a territorial digester), for predicting AD inhibition scenarios, and for optimising the  
492 co-substrate proportions. These improvements will result in an enhanced waste valorisation.  
493 Including competing pathways (*e.g.* AM or SAO as dominant acetate-consuming pathway) has  
494 further practical benefits, since it allows: (i) to account for microbial adaptation without the  
495 need of continuous model recalibration; and (ii) to model microbial shifts (*e.g.* from dominant  
496 AM to HM), which could potentially be used to move away from the traditional operational

497 approach of stopping the reactor feed at minimal VFA increases. We consider that the benefits  
498 of implementing the modified ADM1 presented here outweigh the minor increase in model  
499 complexity. We recommend the application of the modified ADM1 for any AD system where  
500 it is suspected that AM might be inhibited due to high FAN concentrations (*i.e.* over 340 mg  
501 FAN-N·L<sup>-1</sup>, based on Capson-Tojo et al. (2020)). The application of this model is not only  
502 restricted to FW AD, but can also be extended to any FAN-rich reactor, such as manure  
503 digesters. Further work should focus on calibration and validation of the modified ADM1 with  
504 continuous experiments, testing microbial acclimation to FAN and microbial shifts (*e.g.* from  
505 AM to HM).

506 AD models (high-solids models in particular) should account for the non-ideal behaviour of the  
507 solution. Further modifications to include activity corrections for chemical species other than  
508 FAN, or to consider ion pairing, would allow to: (i) improve the pH and model performance  
509 predictions (Solon et al., 2015); (ii) to accurately predict inhibition by other compounds (*e.g.*  
510 H<sub>2</sub>S) (Durán et al., 2020; Patón et al., 2018); and (iii) to model the precise chemical speciation  
511 and complexation of relevant elements (*e.g.* P, S or Fe) (Flores-Alsina et al., 2016). Although  
512 non-ideality considerations are commonly considered by using the Debye-Hückel equation,  
513 fully defined comprehensive chemistry engines (*e.g.* PHREEQC or MINTEQA2) could also be  
514 integrated with AD models (Durán et al., 2020). Ion pairing and activity corrections could be  
515 coupled to a model considering TE complexation and precipitation, which would be particularly  
516 relevant if TEs are dosed in the digesters (Frunzo et al., 2019; Maharaj et al., 2019). Another  
517 potential modification could be to consider the variable TS contents in the reactors. As  
518 explained in Pastor-Poquet et al. (2018), the TS content can change in high-solids AD reactors  
519 due to the conversion of solid organics into biogas (up to around 10% with municipal solid  
520 waste as substrate). Consequently, the concentrations of soluble compounds and solids in the  
521 reactors can be affected. This effect was not considered in this work because the change in

522 volume from the start to the end of the experiments was considered negligible under the  
523 working conditions (estimated at 3-5% reactor volume loss).

524 The accurate prediction of FAN inhibitory limits is relevant, as it allows the compare the  
525 obtained values with those from the literature, and to obtain accurate limits for different  
526 predominant microbial communities. Furthermore, applying a more realistic model can help to  
527 provide a better understanding of FAN inhibition in anaerobic systems and to better predict  
528 microbial community shifts due to inhibition. Proper modelling of FAN-rich systems (including  
529 accurate inhibition limits) would improve the predictions of acetic and propionic acid profiles,  
530 which in turn could be used to better understand the impact of additives (*e.g.* GAC) on AD.  
531 This will not only assist in optimising the dosage and characteristics of these additives but will  
532 also aid to find other alternatives.

533

#### 534 **4. Conclusions**

535 Results showed that the modified ADM1 is a suitable approach to model FW AD. The modified  
536 ADM1 was able to represent the methane production rates and the VFA profiles simultaneously,  
537 which could not be achieved with the default ADM1. The modified model also predicted the  
538 predominant acetate-consuming and methane-producing microbial clades, with SAO and HM  
539 being dominant. A modified Davies equation accurately estimated FAN concentrations, which  
540 improved pH predictions and provided better estimates for inhibition limits. Finally, the  
541 modified model showed that the addition of GAC enhances FW AD by improving the HM  
542 kinetics.

543

#### 544 **E-supplementary material**

545 E-supplementary material for this work can be found in the online version of the paper.

#### 546 **Acknowledgements**

547 Gabriel Capson-Tojo is grateful to the Xunta de Galicia for his postdoctoral fellowship  
548 (ED481B-2018/017). Sergi Astals is thankful to the Spanish Ministry of Science, Innovation  
549 and Universities for his Ramon y Cajal fellowship (RYC-2017-22372). Ángel Robles is grateful  
550 for the support from the Spanish Ministry of Science and Innovation and the Partnership for  
551 Research and Innovation in the Mediterranean Area (Grant PCI2020-112218).

552

553 **References**

- 554 1. Angelidaki, I., Alves, M.M., Bolzonella, D., Borzacconi, L., Campos, J.L., Guwy, A.J.,  
555 Kalyuzhnyi, S., Jenicek, P., Van Lier, J.B., 2009. Defining the biomethane potential  
556 (BMP) of solid organic wastes and energy crops: a proposed protocol for batch assays.  
557 2. APHA, 2017. Standard Methods for the Examination of Water and Wastewater.  
558 American Public Health Association, Washington, DC.  
559 3. Appels, L., Baeyens, J., Degrève, J., Dewil, R., 2008. Principles and potential of the  
560 anaerobic digestion of waste-activated sludge. *Prog. Energy Combust. Sci.* 34, 755–781.  
561 4. Astals, S., Esteban-Gutiérrez, M., Fernández-Arévalo, T., Aymerich, E., García-Heras,  
562 J.L., Mata-Alvarez, J., 2013. Anaerobic digestion of seven different sewage sludges: A  
563 biodegradability and modelling study. *Water Res.* 47, 6033–6043.  
564 5. Astals, S., Peces, M., Batstone, D.J., Jensen, P.D., Tait, S., 2018. Characterising and  
565 modelling free ammonia and ammonium inhibition in anaerobic systems. *Water Res.* 143,  
566 127–135.  
567 6. Banks, C.J., Chesshire, M., Stringfellow, A., 2008. A pilot-scale trial comparing  
568 mesophilic and thermophilic digestion for the stabilisation of source segregated kitchen  
569 waste. *Water Sci. Technol.* 58, 1475–1481.  
570 7. Banks, C.J., Zhang, Y., Jiang, Y., Heaven, S., 2012. Trace element requirements for  
571 stable food waste digestion at elevated ammonia concentrations. *Bioresour. Technol.* 104,  
572 127–135.  
573 8. Barua, S., Dhar, B.R., 2017. Advances Towards Understanding and Engineering Direct  
574 Interspecies Electron Transfer in Anaerobic Digestion. *Bioresour. Technol.* 244, 698–  
575 707.  
576 9. Batstone, D.J., Keller, J., Angelidaki, I., Kalyuzhny, S. V., Pavlostathis, S.G., Rozzi, A.,  
577 Sanders, W.T.M., Siegrist, H., Vavilin, V.A., 2002. Anaerobic digestion model no. 1  
578 (ADM1). IWA Publishing.  
579 10. Campolongo, F., Cariboni, J., Saltelli, A., 2007. An effective screening design for  
580 sensitivity analysis of large models. *Environ. Model. Softw.* 22, 1509–1518.  
581 11. Capson-Tojo, G., Moscoviz, R., Astals, S., Robles, A., Steyer, J.-P., 2020. Unraveling the  
582 literature chaos around free ammonia inhibition in anaerobic digestion. *Renew. Sustain.*  
583 *Energy Rev.* 117, 109487.  
584 12. Capson-Tojo, G., Moscoviz, R., Ruiz, D., Santa-Catalina, G., Trably, E., Rouez, M.,  
585 Crest, M., Steyer, J.-P., Bernet, N., Delgenès, J.-P., Escudíé, R., 2018a. Addition of  
586 granular activated carbon and trace elements to favor volatile fatty acid consumption  
587 during anaerobic digestion of food waste. *Bioresour. Technol.* 260, 157–168.

- 588 13. Capson-Tojo, G., Rouez, M., Crest, M., Steyer, J.-P., Delgenès, J.-P., Escudié, R., 2016.  
589 Food waste valorization via anaerobic processes: a review. *Rev. Environ. Sci.*  
590 *Bio/Technology* 15, 499–547.
- 591 14. Capson-Tojo, G., Ruiz, D., Rouez, M., Crest, M., Steyer, J.-P., Bernet, N., Delgenès, J.-  
592 P., Escudié, R., 2017. Accumulation of propionic acid during consecutive batch anaerobic  
593 digestion of commercial food waste. *Bioresour. Technol.* 245, 724–733.
- 594 15. Capson-Tojo, G., Trably, E., Rouez, M., Crest, M., Bernet, N., Steyer, J.-P., Delgenès, J.-  
595 P., Escudié, R., 2018b. Cardboard proportions and total solids contents as driving factors  
596 in dry co-fermentation of food waste. *Bioresour. Technol.* 248, 229–237.
- 597 16. De Vrieze, J., Saunders, A.M., He, Y., Fang, J., Nielsen, P.H., Verstraete, W., Boon, N.,  
598 2015. Ammonia and temperature determine potential clustering in the anaerobic digestion  
599 microbiome. *Water Res.* 75, 312–323.
- 600 17. Dubois, M., Gilles, K.A., Hamilton, J.K., Rebers, P.A., Smith, F., 1956. Colorimetric  
601 Method for Determination of Sugars and Related Substances. *Anal. Chem.* 28, 350–356.
- 602 18. Durán, F., Robles, Á., Giménez, J.B., Ferrer, J., Ribes, J., Serralta, J., 2020. Modelling  
603 the anaerobic treatment of sulfate-rich urban wastewater: application to AnMBR  
604 technology. *Water Res.* 184, 116133.
- 605 19. Fagbohunge, M.O., Herbert, B.M.J., Hurst, L., Ibeto, C.N., Li, H., Usmani, S.Q.,  
606 Semple, K.T., 2017. The challenges of anaerobic digestion and the role of biochar in  
607 optimizing anaerobic digestion. *Waste Manag.* 61, 236–249.
- 608 20. Flores-Alsina, X., Solon, K., Kazadi Mbamba, C., Tait, S., Gernaey, K. V., Jeppsson, U.,  
609 Batstone, D.J., 2016. Modelling phosphorus (P), sulfur (S) and iron (Fe) interactions for  
610 dynamic simulations of anaerobic digestion processes. *Water Res.* 95, 370–382.
- 611 21. Frunzo, L., Feroso, F.G., Luongo, V., Mattei, M.R., Esposito, G., 2019. ADM1-based  
612 mechanistic model for the role of trace elements in anaerobic digestion processes. *J.*  
613 *Environ. Manage.* 241, 587–602.
- 614 22. Galí, A., Benabdallah, T., Astals, S., Mata-Alvarez, J., 2009. Modified version of ADM1  
615 model for agro-waste application. *Bioresour. Technol.* 100, 2783–2790.
- 616 23. Hafner, S.D., Bisogni, J.J., 2009. Modeling of ammonia speciation in anaerobic digesters.  
617 *Water Res.* 43, 4105–4114.
- 618 24. Hao, L., Michaelsen, T.Y., Singleton, C.M., Dottorini, G., Kirkegaard, R.H., Albertsen,  
619 M., Nielsen, P.H., Dueholm, M.S., 2020. Novel syntrophic bacteria in full-scale  
620 anaerobic digesters revealed by genome-centric metatranscriptomics. *ISME J.* 14, 906–  
621 918.
- 622 25. Jiang, Y., Banks, C., Zhang, Y., Heaven, S., Longhurst, P., 2017. Quantifying the  
623 percentage of methane formation via acetoclastic and syntrophic acetate oxidation  
624 pathways in anaerobic digesters. *Waste Manag.* 71, 749–756.
- 625 26. Karthikeyan, O.P., Visvanathan, C., 2013. Bio-energy recovery from high-solid organic  
626 substrates by dry anaerobic bio-conversion processes: a review. *Rev. Environ. Sci.*  
627 *Bio/Technology* 12, 257–284.
- 628 27. Koch, K., Helmreich, B., Drewes, J.E., 2015. Co-digestion of food waste in municipal  
629 wastewater treatment plants: Effect of different mixtures on methane yield and hydrolysis  
630 rate constant. *Appl. Energy* 137, 250–255.
- 631 28. Maharaj, B.C., Mattei, M.R., Frunzo, L., Hullebusch, E.D. va., Esposito, G., 2019.  
632 ADM1 based mathematical model of trace element complexation in anaerobic digestion  
633 processes. *Bioresour. Technol.* 253–259.
- 634 29. Montecchio, D., Astals, S., Di Castro, V., Gallipoli, A., Gianico, A., Pagliaccia, P.,  
635 Piemonte, V., Rossetti, S., Tonanzi, B., Braguglia, C.M., 2019. Anaerobic co-digestion of

- 636 food waste and waste activated sludge: ADM1 modelling and microbial analysis to gain  
637 insights into the two substrates' synergistic effects. *Waste Manag.* 97, 27–37.
- 638 30. Montecchio, D., Esposito, G., Gagliano, M.C., Gallipoli, A., Gianico, A., Braguglia,  
639 C.M., 2017. Syntrophic acetate oxidation during the two-phase anaerobic digestion of  
640 waste activated sludge: Microbial population, Gibbs free energy and kinetic modelling.  
641 *Int. Biodeterior. Biodegrad.* 125, 177–188.
- 642 31. Morris, M., 1991. Factorial sampling plans for preliminary computational experiments.  
643 *Technometrics* 33, 239–245.
- 644 32. Moscoviz, R., de Fouchécour, F., Santa-Catalina, G., Bernet, N., Trably, E., 2017.  
645 Cooperative growth of *Geobacter sulfurreducens* and *Clostridium pasteurianum* with  
646 subsequent metabolic shift in glycerol fermentation. *Sci. Rep.* 7, 44334.
- 647 33. Motte, J.-C., Escudié, R., Beaufile, N., Steyer, J.-P., Bernet, N., Delgenès, J.-P., Dumas,  
648 C., 2014. Morphological structures of wheat straw strongly impacts its anaerobic  
649 digestion. *Ind. Crops Prod.* 52, 695–701.
- 650 34. Motte, J.-C., Trably, E., Escudié, R., Hamelin, J., Steyer, J.-P., Bernet, N., Delgenes, J.-  
651 P., Dumas, C., 2013. Total solids content: a key parameter of metabolic pathways in dry  
652 anaerobic digestion. *Biotechnol. Biofuels* 6, 164.
- 653 35. Pastor-Poquet, V., Papirio, S., Steyer, J.P., Trably, E., Escudié, R., Esposito, G., 2019.  
654 Modelling non-ideal bio-physical-chemical effects on high-solids anaerobic digestion of  
655 the organic fraction of municipal solid waste. *J. Environ. Manage.* 238, 408–419.
- 656 36. Pastor-Poquet, V., Papirio, S., Steyer, J.P., Trably, E., Escudié, R., Esposito, G., 2018.  
657 High-solids anaerobic digestion model for homogenized reactors. *Water Res.* 142, 501–  
658 511.
- 659 37. Patón, M., González-Cabaleiro, R., Rodríguez, J., 2018. Activity corrections are required  
660 for accurate anaerobic digestion modelling. *Water Sci. Technol.* 77, 2057–2067.
- 661 38. Poggio, D., Walker, M., Nimmo, W., Ma, L., Pourkashanian, M., 2016. Modelling the  
662 anaerobic digestion of solid organic waste - Substrate characterisation method for ADM1  
663 using a combined biochemical and kinetic parameter estimation approach. *Waste Manag.*  
664 53, 40–54.
- 665 39. Rajagopal, R., Massé, D.I., Singh, G., 2013. A critical review on inhibition of anaerobic  
666 digestion process by excess ammonia. *Bioresour. Technol.* 143, 632–641.
- 667 40. Rathnasiri, P.G., 2016. Dynamic Modelling and Simulation of Pilot Scale Anaerobic  
668 Digestion Plant Treating Source Separated Food Waste and Effect of Recycling Sludge.  
669 *Procedia Environ. Sci.* 35, 740–748.
- 670 41. Regmi, P., Miller, M., Jimenez, J., Stewart, H., Johnson, B., Amerlinck, Y., Volcke,  
671 E.I.P., Arnell, M., García, P.J., Maere, T., Torfs, E., Vanrolleghem, P.A., Miletić, I.,  
672 Rieger, L., Schraa, O., Samstag, R., Santoro, D., Snowling, S., Takács, I., 2019. The  
673 future of WRRF modelling - Outlook and challenges. *Water Sci. Technol.* 79, 3–14.
- 674 42. Rivera-Salvador, V., López-Cruz, I.L., Espinosa-Solares, T., Aranda-Barradas, J.S.,  
675 Huber, D.H., Sharma, D., Toledo, J.U., 2014. Application of Anaerobic Digestion Model  
676 No. 1 to describe the syntrophic acetate oxidation of poultry litter in thermophilic  
677 anaerobic digestion. *Bioresour. Technol.* 167, 495–502.
- 678 43. Robles, A., Ruano, M. V., Ribes, J., Seco, A., Ferrer, J., 2014. Global sensitivity analysis  
679 of a filtration model for submerged anaerobic membrane bioreactors (AnMBR).  
680 *Bioresour. Technol.* 158, 365–373.
- 681 44. Rosen, C., Jeppsson, U., 2006. Aspects on ADM1 Implementation within the BSM2  
682 Framework. *Tech. Rep.* 1–37.

- 683 45. Solon, K., Flores-Alsina, X., Mbamba, C.K., Volcke, E.I.P., Tait, S., Batstone, D.,  
 684 Gernaey, K. V., Jeppsson, U., 2015. Effects of ionic strength and ion pairing on (plant-  
 685 wide) modelling of anaerobic digestion. *Water Res.* 70, 235–245.
- 686 46. Stumm, W., Morgan, J.J., 1996. *Aquatic Chemistry: Chemical Equilibria and Rates in*  
 687 *Natural Waters*, 3rd ed. John Wiley & Sons.
- 688 47. Weinrich, S., Nelles, M., 2021. Systematic simplification of the Anaerobic Digestion  
 689 Model No. 1 (ADM1) – Model development and stoichiometric analysis. *Bioresour.*  
 690 *Technol.* 333.
- 691 48. Wett, B., Takács, I., Batstone, D., Wilson, C., Murthy, S., 2014. Anaerobic model for  
 692 high-solids or high-temperature digestion - Additional pathway of acetate oxidation.  
 693 *Water Sci. Technol.* 69, 1634–1640.
- 694 49. Zhao, X., Li, L., Wu, D., Xiao, T., Ma, Y., Peng, X., 2019. Modified Anaerobic  
 695 Digestion Model No. 1 for modeling methane production from food waste in batch and  
 696 semi-continuous anaerobic digestions. *Bioresour. Technol.* 271, 109–117.

## 697 Figure and table captions

698 **Figure 1.** Results of the sensitivity analysis of the control reactor for the five model outputs  
 699 used for calibration (*i.e.* methane flow rate and concentrations of acetate, propionate, butyrate,  
 700 and valerate). Results for both the (A-E) default ADM1 and the (F-J) modified ADM1 are  
 701 presented.

702 **Figure 2.** Experimental data and modelling results corresponding to the methane production  
 703 curves ( $Q_{CH_4}$ ) and the concentrations of acetate, propionate, butyrate, and valerate in the control  
 704 reactor. Modelling results using the (A-F) default ADM1 and the (G-L) modified ADM1 are  
 705 presented. The  $R^2$  given correspond to parity plots.

706 **Figure 3.** Predicted biomass concentrations by (A) the default ADM1 and (B) the modified  
 707 ADM1 with data from the control reactor. The (C) pH and (D) TAN and FAN concentrations  
 708 predicted by both models are also shown.

709 **Figure 4.** Experimental data and modelling results corresponding to the methane production  
 710 curves ( $Q_{CH_4}$ ) and the concentrations of acetate, propionate, butyrate, and valerate for the GAC-  
 711 supplemented reactor. The modelling results for both the (A-F) modified ADM1 and the (G-L)  
 712 default ADM1 are shown. The  $R^2$  given correspond to parity plots.

713 **Table 1.** Main characteristics (average and standard deviations) of the food waste and the  
 714 inoculum.

715 **Table 2.** Calibration results for the control reactor of the relevant parameters in the default and  
 716 the modified ADM1. The results correspond to the control reactor (no additives supplied). The  
 717 values from the ADM1 are given for mesophilic conditions (35 °C).

718 **Table 3.** Calibration results for the control reactor and for reactors supplemented with granular  
 719 activated carbon (GAC). The results from parameters deemed as relevant are shown for both  
 720 the default and the modified ADM1.

721 **Table 4.** Values of uptake rates ( $k_m$ ;  $\text{kg COD}\cdot\text{kg COD}^{-1}\cdot\text{d}^{-1}$ ) related to acetate and hydrogen  
 722 uptake from the literature and in this study.

## 723 Credit author statement

724 Conceptualization was performed by GC-T, SA and AR. GC-T and AR carried out  
 725 methodology, software, and formal analysis. GC-T and SA wrote the original manuscript. GC-  
 726 T, SA and AR carried out manuscript review and editing. Visualisation was performed by GCT.

727 All authors contributed to the article and approved the submitted version.

728

729

730 **Declaration of interest statement**

731 The authors do not have interests to declare.

732

733

734 **Highlights**

735 • The modified ADM1 improved the predicted methane and volatile fatty acids profiles

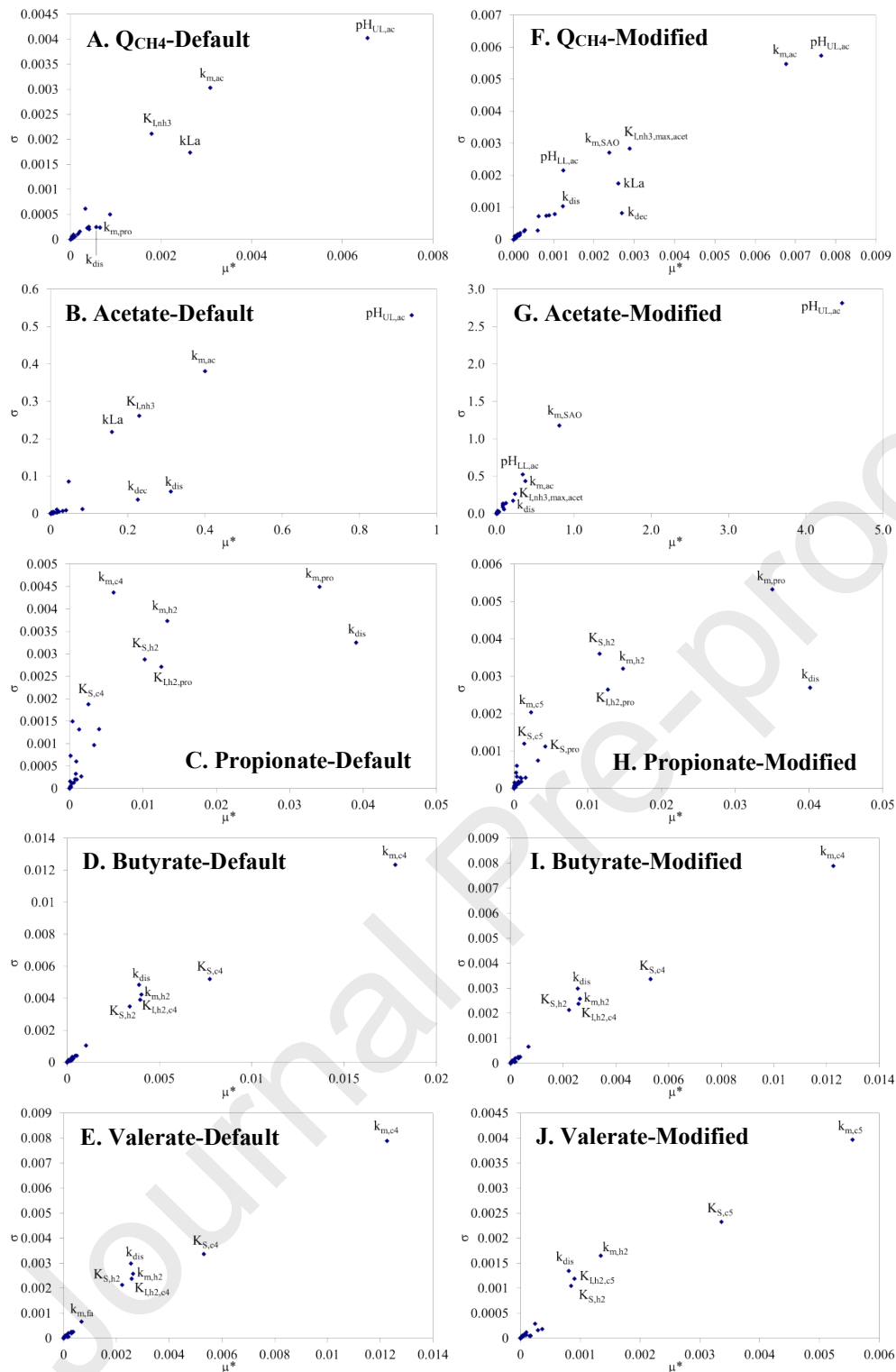
736 • The modified ADM1 enhanced free ammonia estimation and inhibition modelling

737 • The predominant metabolic pathways were adequately predicted

738 •  $k_{La}$  and  $k_{dis}$  were relevant parameters for accurate food waste digestion modelling

739 • Model results showed that granular activated carbon enhanced hydrogen uptake

740



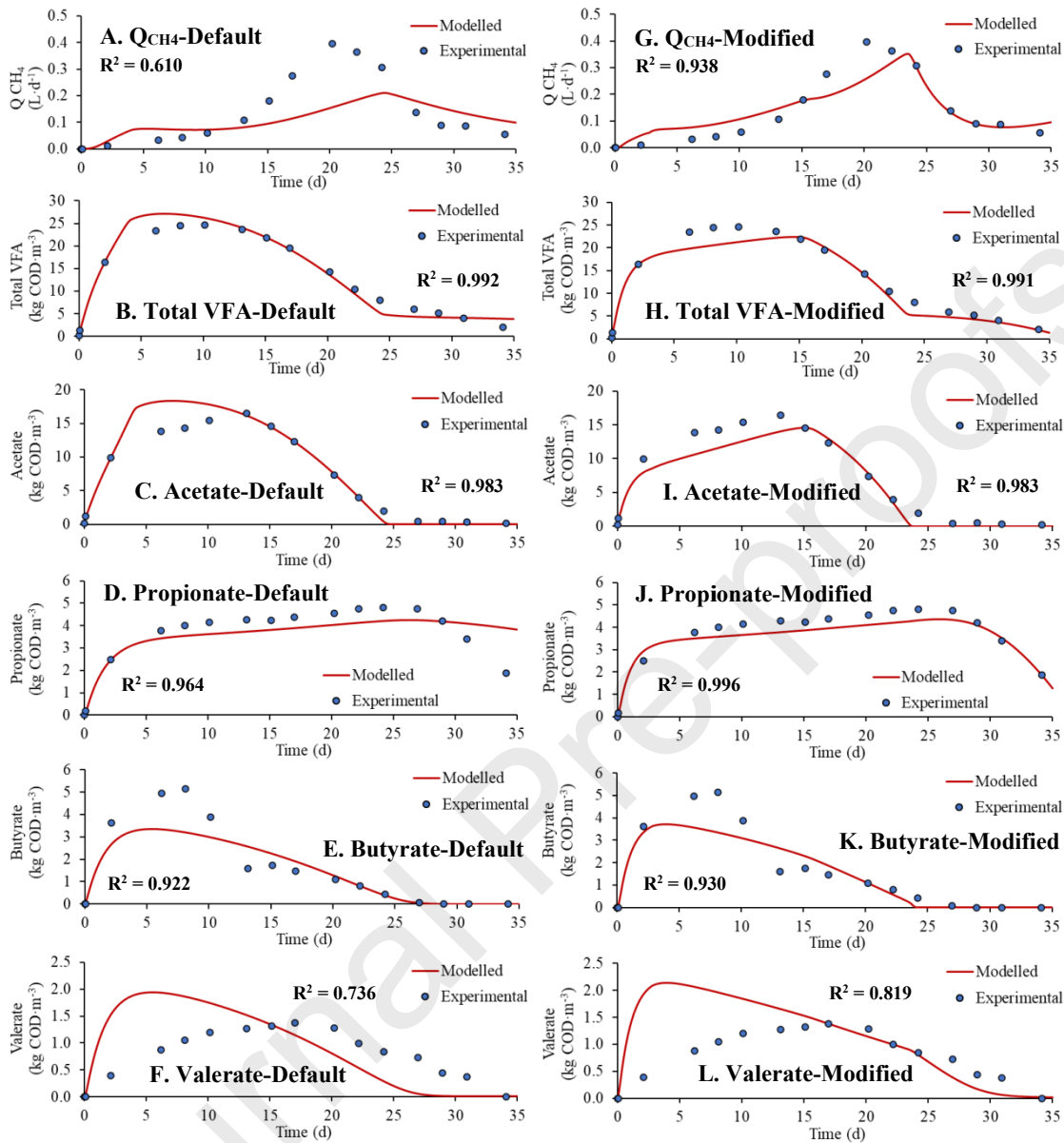
741

742 **Figure 1.** Results of the sensitivity analysis of the control reactor for the five model outputs743 used for calibration (*i.e.* methane flow rate and concentrations of acetate, propionate, butyrate,

744 and valerate). Results for both the (A-E) default ADM1 and the (F-J) modified ADM1 are

745 presented.

746



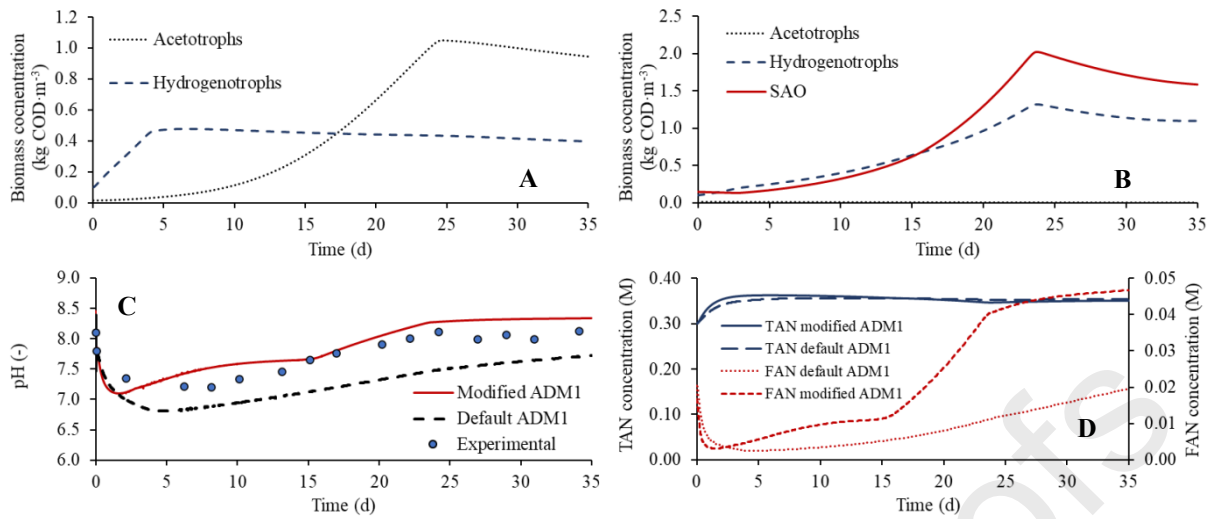
747

748 **Figure 2.** Experimental data and modelling results corresponding to the methane production749 curves ( $Q_{CH_4}$ ) and the concentrations of acetate, propionate, butyrate, and valerate in the control

750 reactor. Modelling results using the (A-F) default ADM1 and the (G-L) modified ADM1 are

751 presented. The  $R^2$  given correspond to parity plots.

752



753

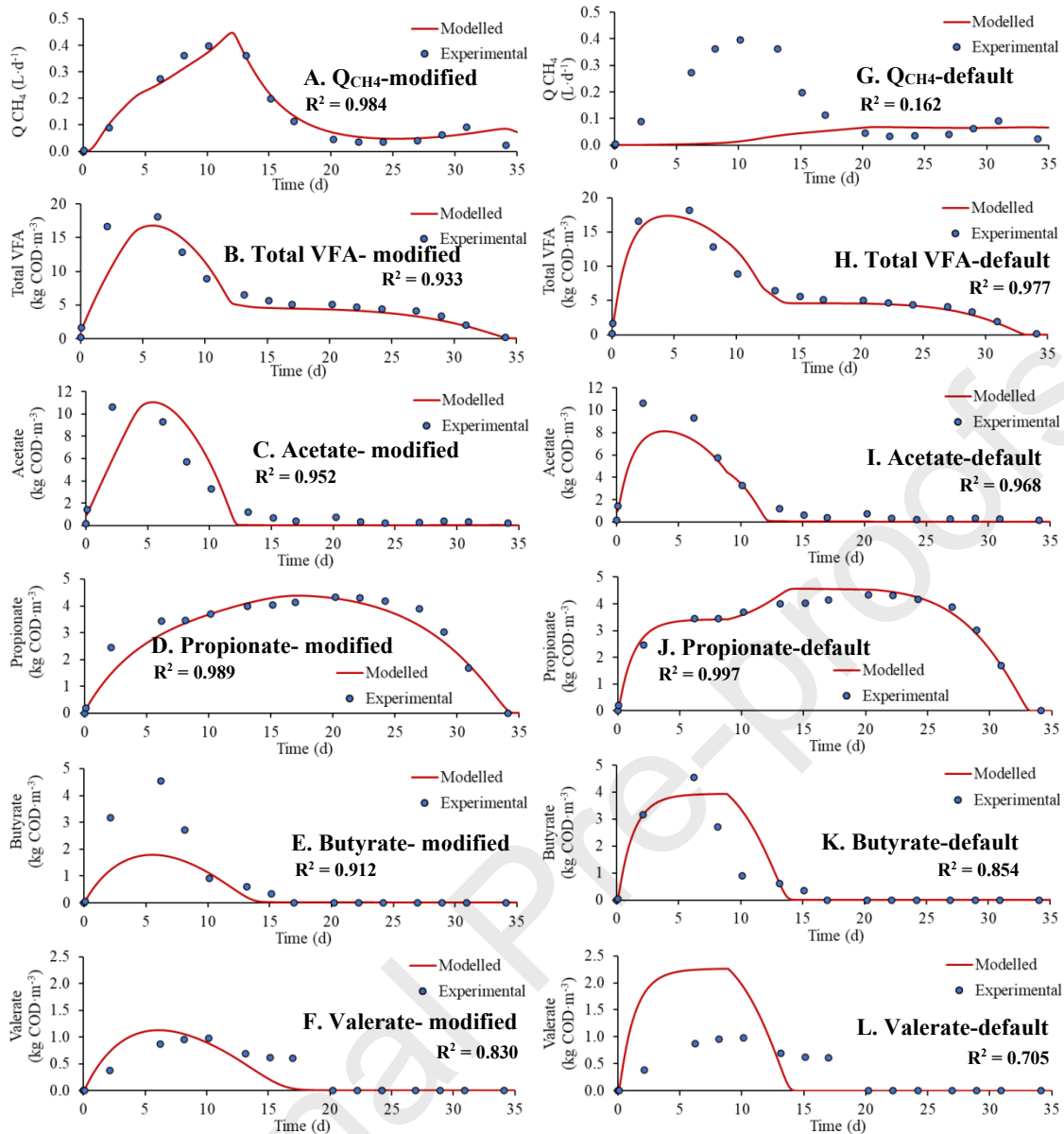
754 **Figure 3.** Predicted biomass concentrations by (A) the default ADM1 and (B) the modified

755 ADM1 with data from the control reactor. The (C) pH and (D) TAN and FAN concentrations

756 predicted by both models are also shown.

757

758



759

760 **Figure 4.** Experimental data and modelling results corresponding to the methane production  
 761 curves ( $Q_{CH_4}$ ) and the concentrations of acetate, propionate, butyrate, and valerate for the GAC-  
 762 supplemented reactor. The modelling results for both the (A-F) modified ADM1 and the (G-L)  
 763 default ADM1 are shown. The  $R^2$  given correspond to parity plots.

764

765 **Table 1.** Main characteristics (average and standard deviations) of the food waste and the  
 766 inoculum.

Parameter	Food waste mixture	Inoculum
-----------	--------------------	----------

TS (%)	21.0 ± 0.36	6.14 ± 0.62
VS/TS (%)	90.3 ± 0.76	56.8 ± 3.56
Carbohydrates (g·kg TS <sup>-1</sup> )	618 ± 23	n.m.
Proteins (g·kg TS <sup>-1</sup> )	187 ± 10	n.m.
Lipids (g·kg TS <sup>-1</sup> )	121 ± 21	n.m.
BMPs (mL CH <sub>4</sub> ·g VS <sup>-1</sup> )	420 ± 5.28	n.m.
pH	5.02 ± 0.18	8.10 ± 0.10
TAN (g N·L <sup>-1</sup> )	0.90 ± 0.72	7.27 ± 0.51
TKN (g N·kg TS <sup>-1</sup> )	30.0 ± 1.64	n.m.

767 TS stands for total solids, VS for volatile solids, n.m. for “not measured”, BMP for biochemical methane potential,  
 768 TAN for total ammonia nitrogen, and TKN for total Kjeldahl nitrogen  
 769

770  
 771 **Table 2.** Calibration results for the control reactor of the relevant parameters in the default and  
 772 the modified ADM1. The results correspond to the control reactor (no additives supplied). The  
 773 values from the ADM1 are given for mesophilic conditions (35 °C).

Symbol	Parameter	Units	Default value	Source	Calibration results	
					Default ADM1	Modified ADM1
$k_{dis}$	First order disintegration rate	g COD·g COD <sup>-1</sup> ·d <sup>-1</sup>	0.5	(Batstone et al., 2002)	0.606	0.975
$k_{La}$	Mass transfer coefficient	d <sup>-1</sup>	200	(Rosen and Jeppsson, 2006)	0.087	0.390
$k_{m,ac}$	Acetate uptake rate by methanogens	g COD·g COD <sup>-1</sup> ·d <sup>-1</sup>	8	(Batstone et al., 2002)	10.74	1.292
$k_{m,pro}$	Propionate uptake rate	g COD·g COD <sup>-1</sup> ·d <sup>-1</sup>	13	(Batstone et al., 2002)	2.926	19.21
$k_{m,h2}$	Hydrogen uptake rate	g COD·g COD <sup>-1</sup> ·d <sup>-1</sup>	35	(Batstone et al., 2002)	21.82	4.684
$k_{m,e4}$	Butyrate/valerate uptake rate <sup>1</sup>	g COD·g COD <sup>-1</sup> ·d <sup>-1</sup>	20	(Batstone et al., 2002)	1.494	7.147
$k_{m,e5}$	Valerate uptake rate	g COD·g COD <sup>-1</sup> ·d <sup>-1</sup>	20	(Batstone et al., 2002)	-	2.894
$k_{m,SAO}$	Acetate uptake rate by SAO	g COD·g COD <sup>-1</sup> ·d <sup>-1</sup>	3.25	(Rivera-Salvador et al., 2014)	-	4.851
$k_{dec}$	First order biomass decay rate	g COD·g COD <sup>-1</sup> ·d <sup>-1</sup>	0.02	(Batstone et al., 2002)	0.015	0.039
$K_{S,e4}$	Half saturation constant for butyrate/valerate <sup>1</sup>	mg COD·L <sup>-1</sup>	0.2	(Batstone et al., 2002)	0.237	0.075
$K_{S,e5}$	Half saturation constant for valerate	mg COD·L <sup>-1</sup>	0.2	(Batstone et al., 2002)	-	0.390
$K_{S,h2}$	Half saturation constant for hydrogen	mg COD·L <sup>-1</sup>	7·10 <sup>-6</sup>	(Batstone et al., 2002)	3.2·10 <sup>-6</sup>	1.2·10 <sup>-5</sup>
$K_{I,h2,e4}$	H <sub>2</sub> 50% inhibitory concentration for	mg COD·L <sup>-1</sup>	1·10 <sup>-5</sup>	(Batstone et al., 2002)	1.9·10 <sup>-5</sup>	2.9·10 <sup>-6</sup>

butyrate/valerate uptake <sup>1</sup>						
$K_{I,h2,c5}$	H <sub>2</sub> 50% inhibitory concentration for valerate uptake	mg COD·L <sup>-1</sup>	1·10 <sup>-5</sup>	(Batstone et al., 2002)	-	8.4·10 <sup>-6</sup>
$K_{I,h2,pro}$	H <sub>2</sub> 50% inhibitory concentration for propionate uptake	mg COD·L <sup>-1</sup>	3.5·10 <sup>-6</sup>	(Batstone et al., 2002)	2.4·10 <sup>-7</sup>	9.6·10 <sup>-7</sup>
$K_{I,NH3}$	NH <sub>3</sub> 50% inhibitory concentration for acetate uptake by methanogens	M	0.0018	(Batstone et al., 2002)	0.0030	-
$K_{I,NH3,max,acet}$	FAN concentrations where inhibition of acetate uptake by methanogens is almost complete	M	0.0109	(Capson-Tojo et al., 2020)	-	0.011
$pH_{UL,ac}$	50% pH upper limit for acetotrophs	-	7	(Batstone et al., 2002)	7.12	-

774 SAO stands for syntrophic acetate oxidation and FAN for free ammonia nitrogen.

775 1. Valerate only in the default ADM1

776

777

778 **Table 3.** Calibration results for the control reactor and for reactors supplemented with granular

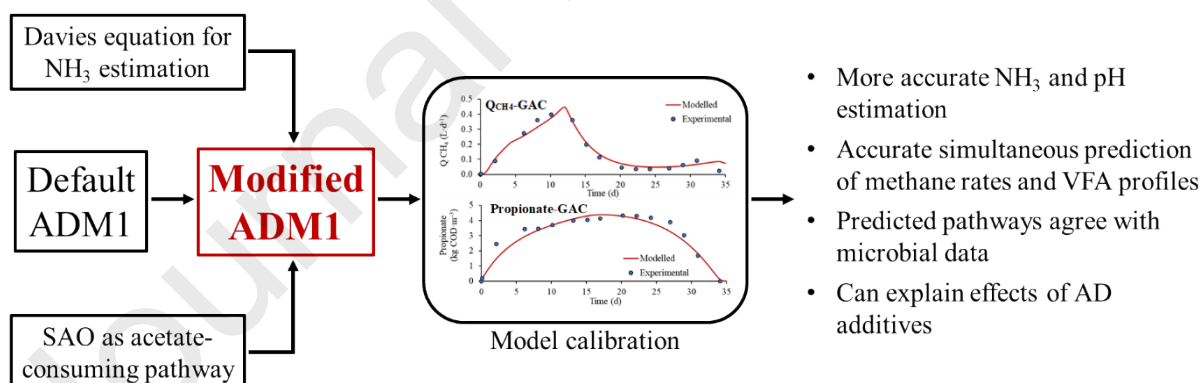
779 activated carbon (GAC). The results from parameters deemed as relevant are shown for both

780 the default and the modified ADM1.

Parameter	Units	Default ADM1		Modified ADM1	
		Control	GAC	Control	GAC
$k_{dis}$	g COD·g COD <sup>-1</sup> ·d <sup>-1</sup>	0.606	0.802	0.975	0.236
$k_{m,ac}$	g COD·g COD <sup>-1</sup> ·d <sup>-1</sup>	10.74	14.68	1.291	3.864
$k_{m,pro}$	g COD·g COD <sup>-1</sup> ·d <sup>-1</sup>	2.93	9.55	19.21	5.927
$k_{m,h2}$	g COD·g COD <sup>-1</sup> ·d <sup>-1</sup>	21.8	1.75	4.684	24.295
$k_{m,c4}$	g COD·g COD <sup>-1</sup> ·d <sup>-1</sup>	1.49	22.2	7.147	2.261
$k_{m,c5}$	g COD·g COD <sup>-1</sup> ·d <sup>-1</sup>	-	-	2.894	1.945
$k_{m,SAO}$	g COD·g COD <sup>-1</sup> ·d <sup>-1</sup>	-	-	4.851	3.125
$k_{dec}$	g COD·g COD <sup>-1</sup> ·d <sup>-1</sup>	0.015	0.009	0.039	0.039
$K_{S,c4}$	mg COD·L <sup>-1</sup>	0.237	0.389	0.075	0.138
$K_{S,c5}$	mg COD·L <sup>-1</sup>	-	-	0.390	0.234
$K_{S,h2}$	mg COD·L <sup>-1</sup>	3.2·10 <sup>-6</sup>	4.5·10 <sup>-6</sup>	1.2·10 <sup>-5</sup>	7.2·10 <sup>-6</sup>
$K_{I,h2,c4}$	mg COD·L <sup>-1</sup>	1.9·10 <sup>-5</sup>	1.1·10 <sup>-5</sup>	2.9·10 <sup>-6</sup>	1.5·10 <sup>-5</sup>
$K_{I,h2,c5}$	mg COD·L <sup>-1</sup>	-	-	8.4·10 <sup>-6</sup>	1.9·10 <sup>-5</sup>
$K_{I,h2,pro}$	mg COD·L <sup>-1</sup>	2.4·10 <sup>-7</sup>	4.0·10 <sup>-6</sup>	9.6·10 <sup>-7</sup>	1.0·10 <sup>-6</sup>
$K_{I,NH3}$	M	0.0030	0.0030	-	-
$K_{I,NH3,max,acet}$	M	-	-	0.011	0.010
$pH_{UL,ac}$	-	7.1	6.4	-	-
$k_{I,a}$	d <sup>-1</sup>	0.087	0.016	0.390	0.374

781  
782783  
784 **Table 4.** Values of uptake rates ( $k_m$ ;  $\text{kg COD}\cdot\text{kg COD}^{-1}\cdot\text{d}^{-1}$ ) related to acetate and hydrogen  
785 uptake from the literature and in this study.

Reference	Substrate	SAO	AM	HM
(Rivera-Salvador et al., 2014)	Poultry litter	1.12	-	13
(Montecchio et al., 2017)	Sludge	7	-	70
(Wett et al., 2014)	Sludge	2.6	0.3	-
(Dwyer et al., 1988)	Butyrate and others	0.037-25.0	-	-
Default ADM1	-	-	16	35
This study (default ADM1)	FW	-	10.7-14.7	1.75-21.8
This study (modified ADM1)	FW	3.13-4.85	1.29-3.86	4.68-24.3

786 FW stands for food waste, SAO for syntrophic acetate oxidation, AM for acetoclastic methanogenesis, and HM  
787 for hydrogenotrophic methanogenesis.788  
789**Graphical abstract**790  
791  
792